Study on shear properties of riveted lap joints of aircraft fuselage with different hole diameters

Ming Li
Nanjing University of Aeronautics and Astronautics
Wei Tian (tw_nj@nuaa.edu.cn)
Nanjing University of Aeronautics and Astronautics https://orcid.org/0000-0001-7963-0619
Wenhe Liao
Nanjing University of Aeronautics and Astronautics
Junshan Hu
Nanjing University of Aeronautics and Astronautics
Changrui Wang
Nanjing University of Aeronautics and Astronautics

Research Article

Keywords: riveting, shear properties, aircraft components, hole diameters, lap joint

Posted Date: February 24th, 2021

DOI: https://doi.org/10.21203/rs.3.rs-234041/v1

Abstract

Riveting is the most important way to connect metal sheets, which is widely used in the connection of aircraft components. In this paper, the effect of different hole diameters on the shear properties of riveted lap joints were studied from the perspective of practical application. Considering the symmetry and the calculation time of the model, a 2D axisymmetric finite element method is established with the help of ABAQUS commercial finite element software, the validity of the finite element model is verified by experiment tests. Because the interference distribution has an important influence on the mechanical properties of riveted lap joints, the interference distribution and material flow characteristics in riveting process are analyzed in detail by using finite element method, and the shear characteristics of riveted lap joints in tensile process are explained. The variation of hole diameter with shear force under different squeeze force was obtained by shear test in order to explain the effect of hole diameter on the shear mechanical properties of riveted lap joint. In addition, the fracture mode and microstructure of the rivet shank were characterized by SEM and the formation process of brittleness and plastic fracture is discussed. Finally, the shear failure mechanism of riveted lap joint is analyzed in detail to provide guidance for engineering application. The test results show that all the specimens are both brittle and plastic mixed fracture modes of rivet shank, and the shear strength of the rivet increases with the increase of the hole diameter. Compared with increasing the squeeze force, increasing the hole diameter can effectively improve the shear strength of the riveted lap joint.

1. Introduction

Aircraft assembly is the most important part of the field of modern aircraft manufacturing. Usually, an aircraft is composed of many components. The assembly between components inevitably adopts various connection technologies, including riveting [1-6], bolt connection [7-12], welding [13,14], bonding [15,16] and so on. Among them, riveting is still the main connection method, especially the connection of metal components [17], such as skin, bulkhead, longeron, etc. Compared with riveting, other connection methods have their disadvantages, for example, the processing and manufacturing cost of bolting is high, the welding is non-removable, the bonding quality is unstable. Although riveted joints are widely used in aircraft assembly, the mechanical properties of riveted lap joints are greatly affected by the process parameters of drilling and riveting [18-39]. The good mechanical properties of riveted lap joints are an important guarantee for aircraft service safety.

Due to the advantages of riveting, many scholars have studied the mechanical properties of riveted lap joints. In the study of the effect of riveting process parameters on the fatigue life of riveted lap joints, squeeze force is usually considered as a basic factor, which not only determines the final geometry of the rivet driven head, but also determines the complex residual stress field of the inside and around the rivet/hole. Based on the exponential hardening rule of plastic deformation and the principle of constant volume assumption, an analytical model of the relationship between squeeze force and rivet driven head size is established, which is a means to study the fatigue performance of riveted aircraft structure [17-21]. The riveting quality can be measured by controlling the rivet driven head dimension, due to different rivet

driven head dimensions corresponding to different mechanical properties [22]. The effect of different rivet driven head dimensions on the fatigue life of riveted lap joints was studied by experiment, and the fatigue life was predicted. The results show that different shapes of cracks and different crack propagation paths will appear in the riveted lap joints with different rivet driven head sizes [4,23-24]. The factors related to production variables also have an important influence on the fatigue life of riveted lap joints [25-31]. The interference increases with the increase of squeeze force, for any type of rivet. The interference distribution can be changed by changing the shape of the rivet, and then the fatigue life of riveted lap joints is improved [25-28]. In general, the interference distribution of the universal head rivet in the thickness direction is more uniform and the interference is larger compared with countersunk rivet [29]. Therefore, the universal head rivet will have a greater fatigue life in the case of the same rivet diameter. Besides, the number of rivet rows, row spacing, and sheet thickness also have an important effect on the fatigue life of riveted lap joints [30]. Generally, with the same rivet spacing, the fatigue strength of riveted lap joints increases with the increase of rivet row number, which is mainly due to the decrease of secondary bending caused by large rivet row spacing. However, the overlap area increases, and the weight of the lap joint increases correspondingly with the increase of row spacing, which is extremely unfavorable for aircraft weight reduction. For the thin sheet, increasing the extrusion force can obviously increase the fatigue life. However, the life increase caused by large squeeze force gradually disappears with the increase of sheet thickness [31]. In order to study the influence of different riveting methods on the mechanical properties of riveted lap joints, conventional press riveting and electromagnetic riveting were compared [32]. There is little effect of the riveting method on the shear strength of riveted lap joint, but the difference in fatigue life is significant. The two riveting methods have a significant effect on the fatigue fracture position under different cyclic stresses. Besides, the influence of the environment on aircraft service can not be ignored, Jaya [33] studied the effect of corrosion inhibitor on the fatigue life of riveted lap joints of universal rivets and countersunk rivets by experiments. Furthermore, the joint slip and the stress state around the rivet hole are analyzed by finite element simulation, it is concluded that the fatigue life of the two types of rivets is related to the external load and slip threshold.

Literature review shows that many scholars have conducted extensive research on the production variables, design variables, load types, service environment, and so on in order to improve the mechanical properties of riveted lap joints, which affect the fatigue properties of lap joints. Many scholars have also studied the influence of hole defects and hole quality index on the fatigue life of riveted lap joints. Atre et al. [34] analyzed the fatigue life of baseline specimen and underdriven specimen with the help of the finite element method. It is concluded that fretting is not the only reason for crack initiation, and the influence of hole quality may be the main factor for crack initiation. Zeng et al. [35] established an analytical model of interface pressure affected by initial fit tolerance and squeeze force, and the distribution of residual stress around the hole was studied by finite element method, it is concluded that the effect of tolerance on the residual stress is more significant than that of squeeze force. Furthermore, Zeng et al. [36] studied the comprehensive influence of fit tolerance and squeeze force on the fatigue life of riveted lap joints through fatigue test, and found that the interference fit is not conducive to the

improvement of fatigue life, and the influence of tensile force on the fatigue life of riveted lap joints is more significant than that of fit tolerance. Atre et al. [37] and Sławinski et al. [38] have studied the influence of geometric defects on the fatigue performance of riveted structures by the finite element method. The mismatched rivet holes increase the asymmetric deformation of rivets and lead to the non-uniform compressive residual stress due to the non-uniformity of the interference between the upper and lower skin.

Literature review shows that there are few studies on the effect of hole diameter on the shear mechanical properties of riveted lap joints. The hole diameter has an important influence on the fatigue strength of riveted lap joints [39], the selection of initial hole diameter is related to squeeze force, rivet diameter, and rivet length [20]. In particular, with the explosive growth of the demand for the new generation of civil aircraft and fighters, as well as the demand for long life and high mobility, higher requirements are put forward for assembly quality. In aircraft structural design, ensuring a good static strength threshold is an important guarantee to improve the service performance of aircraft, and also provides basic parameters for fatigue design.

The purpose of this paper is to study the effect of different hole diameters on the shear properties of riveted lap joints. Firstly, the finite element model of the riveting process is established, and the validity of the model is verified. The influence of different hole diameters on the dimensions of rivet driven head and interference distribution was studied by finite element simulation, and the material flow characteristics in the riveting process were further analyzed. The maximum shear load was obtained by shear test, and the shear behavior of riveted lap joint under quasi-static loading was studied. The fracture mode and microstructure of the rivet were characterized by SEM. Finally, the shear failure mechanism of riveted lap joint is analyzed to ensure service safety and provide guidance for engineering application.

2. Materials And Methods

2.1 Specimen preparation

In this study, the shear specimen is made of 2024-T3 aluminum alloy sheet and MS20470 AD6-7 aluminum alloy rivet which is widely used in the skin structure, providing superior performance including high strength, moderate toughness, and corrosion resistance. The thickness of aluminum alloy sheets is 2 mm. The nominal diameter of the rivet is 4.76 mm and the length of the rivet shank is 11.1 mm. The mechanical properties of 2117-T4 and 2024-T3 aluminum alloys are shown in Table 1 [39,40]. In order to eliminate the influence of specimen fixture on the stress condition in the stacking area, the sheet size is set as 174 mm × 24 mm, in which the stacking area size is 24 mm × 24 mm and the clamping area size is 50 mm × 24 mm. The sheets are cut by a wire cutting machine, and the cutting mode of the sheets should make the loading direction parallel to the grain direction of the sheets. Metal gaskets with the same thickness as the sheets are installed at the ends of all specimens to avoid the bending of specimens under shear load. The shear specimens are designed with a single rivet lap joint structure, as depicted in Fig. 1, in which the rivet end distance (m) is 12 mm and the rivet edge distance (n) is 12 mm.

The length of the free end is 10 times the sheet's thickness (t) to ensure that the stress in the rivet is independent of this dimension of the model.

Table 1 Mechanical properties for 2117-T4 and 2024-T3 Al alloy

Material	E (GPa)	σ_s (MPa)	n	C (MPa)	m	K_h (MPa)	ε_{true}	Hardening type
2117-T4	71.7	172	0.33	544	0.23	-	$0.02 \le \varepsilon_{true} \le 0.10$	exponential
				551	0.15		$0.10 \le \varepsilon_{true} \le 1.0$	
2024-T3	72.4	310	0.33	676	0.14		$\varepsilon_s \le \varepsilon_{true} \le 0.02$	
				745	0.164		$0.02 \le \varepsilon_{true} \le 0.10$	
				-	-	1034	$0.10 \le \varepsilon_{true} \le 1.0$	linear

In the process of drilling, a special fixture is used to clamp the laminated sheet to ensure the accuracy of hole position and the quality of the hole. The drilling test platform is shown in Fig. 2. The drilling experiment was completed in Dexi vertical machining center. The spindle speed was 3000 rpm and the feed rate was 120 mm/min, the cutting tool was cemented carbide tri-point drill.

2.2 Riveting test

The riveting experiment is completed on the automatic riveting experiment platform. The riveting machine has two methods of displacement control and force control. Among them, the displacement mode is usually easily affected by the machine structure, the force control mode is the most commonly used, and the fatigue dispersion after riveting is small [23,24]. In the current test, the force control mode is used. Therefore, the squeeze force F_{sq} is selected as the input parameter to obtain the required dimensions of rivet driven head. In this paper, the squeeze force is set at two levels of 15 KN and 23 KN, and the hole diameter is set at five levels of, 4.90 mm, 4.94 mm, 5.00 mm, and 5.10 mm. Each specimen is repeated five times. The detailed experimental setup is shown in Table 2. To easily describe the test configuration of the riveted lap joints the following nomenclature is used: D4.82-F15-NO.X representative diameter of the hole is 4.82 mm and squeeze force is 15 KN, NO.X representative specimen label, the value of X is from 1 to 5.

Table 2 The test configuration of the riveted lap joints and their corresponding specimen group

Test configurations		Squeeze force (F_{sq})	
		15 KN	23 KN
Diameter of hole (D)	4.82mm	D4.82-F15-NO.X	D4.82-F23-NO.X
	4.90 mm	D4.90-F15-NO.X	D4.90-F23-NO.X
	4.94 mm	D4.94-F15-NO.X	D4.94-F23-NO.X
	5.00 mm	D5.00-F15-NO.X	D5.00-F23-NO.X
	5.10 mm	D5.10-F15-NO.X	D5.10-F23-NO.X

2.3 Shear property test

The quasi-static shear test was carried out on a UTM5504Y electronic universal testing machine produced by Sansi Zongheng Technology Co., Ltd. The maximum test force of the testing machine is 50

kN, the whole test operation is carried out at room temperature, and the tensile rate of the uniaxial tensile test is set at 2 mm/min. The fracture morphology of shear test was characterized by FEI Quanta 200 scanning electron microscope. All specimens were cleaned by ultrasonic before the test.

3. Finite Element Analysis

3.1 Finite element models

Considering the symmetry and the calculation time of the model, a 2D axisymmetric finite element method is established, as shown in Fig. 3. The structure of riveted lap joints is composed of five parts, of which two-lap sheets and one rivet are deformable bodies, the rigid bucking bar and rigid set are constrained as rigid bodies. The detailed material parameters are shown in Table 1. The current model includes five contact pairs, as shown by the purple line in the figure. The contact between the rivet and outer sheet, rivet and inner sheet, rivet and rigid bucking bar, rivet and rigid set, and inner sheet and outer sheet are defined respectively. The surface-to-surface explicit contact type is selected for analysis, and the friction coefficient of each contact interface is 0.2 [37,41,42]. The default "hard" contact model is used to simulate normal interaction, and the "finite slip" formula is used to consider relative surface slip. The reduced integral explicit axisymmetric stress element CAX4R is selected as the mesh element, and the enhanced hourglass control is used to avoid the possible zero energy deformation mode. In order to reduce the mesh distortion of rivets and maintain high-quality mesh in the whole analysis process, Arbitrary Lagrange Eulerian (ALE) adaptive mesh technology is also used in the simulation of the riveting process. The finite element analysis of riveted specimens can be divided into three stages: (a) rivet loading, (b) pressure maintenance, (c) rivet unloading. The riveting process is very complicated due to its nonlinear characteristics, so the Nlgeom option is selected [17]. The boundary conditions of the riveting process are set as follows:

(i) The rivet is an axisymmetric structure, which was constrained for displacement along the X direction and rotation along the Z axes.

(ii) Both the right side of the inner sheet and outer sheet were constrained for displacement along with the X and Y directions, and the rotation of Z axes.

(iii) The rigid set was constrained for translation in X and Y directions, and the rotation of Z axes in the rivet loading process. The translation of Y direction was canceled and the displacement is applied in the rivet unloading process.

(iv) The rigid bucking bar was constrained for the translation in the X direction and the rotation of Z axes. The squeeze force is applied in Y- direction during the rivet loading process and the reverse displacement is applied during the rivet unloading process.

3.2 Verification of the finite element model

In the riveting process, the residual stress distribution under the rivet head in the thickness direction and the material flow characteristics of the rivet shank can not be observed directly, so the finite element simulation becomes a powerful tool to analyze the above characteristics. However, the accuracy of finite element simulation affects the accuracy of analysis results. Due to the riveting process is a quasi-static compression process, the inertia effect is usually ignored. Therefore, the ratio of kinetic energy to internal energy in the whole process should not exceed 10%, and the ratio of hourglass energy to internal energy should not exceed 5% in order to ensure good calculation accuracy [37,43]. Fig. 4 shows the comparative analysis of energy curves under the condition of 15 KN and 23 KN squeeze forces. As the graph indicate that the maximum value appears at the beginning of the riveting process, and then rapidly drops to a very low level. The maximum value of the energy curve is within the specified range, so the accuracy of the simulation results can be ensured. The validity of the finite element simulation is verified by measuring the dimensions of rivet driven head. Many kinds of literature and experimental results have described that the dimensions of rivet driven head is an important factor affecting the mechanical properties of riveted lap joints [19,23,25]. Because the dimensions of rivet driven head can be measured intuitively, some aircraft manufacturers have taken the ratio of driven head diameter to rivet shank diameter as the first standard of riveting quality control and specified that D_{dh}/d_0 (D_{dh} represent the diameter of rivet driven head, d_0 is the diameter of rivet shank) should be in the range of 1.3~1.8 [44].

The final deformed of rivet driven head diameter and the final deformed of rivet driven head height by experimental measurements were compared with the finite element simulation results for the specified range of squeeze forces, as shown in Fig. 5. It should be noticed from Fig. 5 that there is no nonlinear relationship between rivet driven head dimension and squeeze force, the diameter of rivet driven head increases, and the height of rivet driven head decreases with the increase of squeeze force. The increased amplitude of rivet diameter decreases when the squeeze force increases to a certain value, which is mainly because the riveting process is a large plastic deformation process accompanied by strain hardening, and the material's ability to resist deformation is enhanced. If larger rivet driven head diameter and smaller rivet driven head height are to be obtained, greater squeeze force will be needed. Besides, it can also be seen that the measured value of rivet driven head diameter is always greater than the finite element simulation value, and the fitting curve of rivet driven head height measurement value and finite element fitting curve intersect. The error comparison between the experimental measurement value and the finite element simulation value under different squeeze forces is shown in Table 3. The maximum error of rivet driven head diameter is 2.13% and the minimum error of rivet driven head diameter is 0.72%, the maximum error of rivet driven head height is 2.29% and the minimum error of rivet driven head height is 0.1%. Many potential factors leading to the difference between the finite element results and the experimental results, such as the change of local material properties due to the different grain size and direction of the material, the error of rivet geometric size and sheet thickness, the constraint conditions, and the experimental measurement error, etc. In general, the experimental results are in good agreement with the simulation results.

Table 3 Dimension error of rivet driven head between finite element and experiment

Experimental variables		Squeeze force (F_{sq})						
		13KN	14KN	15KN	16KN	17KN	18KN	19KN
Rivet driven head dimension	D	1.25	0.78	0.89	1.40	2.13	1.85	1.66
	H	0.22	0.29	-1.02	-1.11	-1.58	-1.53	-1.99
		20KN	21KN	22KN	23KN	24KN	25KN	
	D	1.49	1.94	0.72	1.20	1.50	0.94	
	H	-2.29	-0.76	-0.10	-0.89	-0.31	-1.64	

4. Results And Discussion

4.1 Effect of hole diameter on rivet driven head dimension

The relationship between rivet driven head dimension and hole diameter under different squeeze forces is illustrated in Fig. 6. It can be seen from Fig. 6a that the influence of hole diameter on rivet head diameter is very small under the conditions of 15 KN and 23 KN squeeze force. The height of the driven head decreases along with the increase of hole diameter, especially under the condition of 23 KN squeeze force, but the decreasing amplitude is very small, see Fig. 6b. It can be concluded that the influence of the hole diameter on the rivet driven head dimension is very small under the same squeeze force. Therefore, there are limitations in using rivet driven head dimensions to evaluate riveting quality, which is consistent with the conclusion of Lei [45] and Skorupa [25].

4.2 Influence of hole diameter on interference distribution and material flow characteristics

Interference is another parameter to evaluate the riveting quality, which has an important influence on the mechanical properties of riveted joints. In the process of riveting, the interference can be expressed as absolute interference and relative interference. The absolute interference is the ratio of twice the radial displacement of the hole wall and the hole diameter. However, the relative interference is the ratio of the difference between the rivet shank diameter before and after riveting and the rivet shank diameter before riveting. The absolute interference and relative interference are shown in Eq. (1) and (2) respectively.

$$I = \frac{2\Delta_{\mathrm{H}}}{d_{\mathrm{H}}} \times 100\% \quad (1)$$

$$I = \frac{d - d_0}{d_0} \times 100\% \quad (2)$$

Where Δ_H is the radial displacement of the hole wall after riveting, d_H is the diameter of the rivet hole before riveting, d is the diameter of the rivet shank after riveting, d_0 is the diameter of rivet shank before riveting.

Fig. 7 shows the degree of hole expansion in different hole diameters ranges from 15 KN to 23 KN squeeze force. The left side of the vertical line represents the outer sheet, and the right side represents the inner sheet. It can be seen from the figure that the expansion degree of the inner sheet is greater than that of the outer sheet under each hole diameter, and the difference of hole wall expansion between inner and outer sheets increases with the increase of the squeeze force. There is little difference in the expansion level of the outer sheet along the thickness direction under different hole diameters. However, the

difference of hole expansion level of inner sheet increases, especially near the rivet driven head side. The expansion degree of the hole wall on the side of the rivet driven head is greater than that on the side of the rivet manufactured head, whether it is 15 KN or 23 KN squeeze force. The above phenomena are related to the material flow characteristics during riveting.

Generally, the rivet and hole belong to clearance fit in the initial state, and the diameter of the hole is larger than the diameter of the rivet shank. In the early stage of the riveting process, the whole rivet shank belongs to the free upsetting stage when the rivet shank does not contact the hole wall, and the material mainly flows in the axial direction. The radial expansion of the rivet shank is limited by the hole wall when the rivet shank contacts with the hole wall and the axial material flow of the rivet shank tend to be saturated. Only a small amount of material will flow into the hole under the action of squeeze force, the remaining material in the rivet shank will form the rivet driven head. The axial path of rivet shank at different radial positions is shown in Fig. 3. The change of radial displacement under different paths is illustrated in Fig. 8. In the figure, the left side of the vertical line represents inside the hole and the right side represents outside the hole. As the figure shows, the radial displacement of the rivet shank inside the hole has little change, and the increase of radial displacement mainly occurs outside the hole. The radial displacement of the rivet near the surface outside the hole first increases and then decreases, which is caused by the uneven distribution of friction in the forming process of rivet driven head. The radial displacement of 23 KN squeeze force is greater than that of 15 KN squeeze force under the same path condition. The radial displacement values of different paths are significantly different, and the radial displacement value of path 1 is the largest, and the radial displacement value of path 4 is the smallest. The mutation points of radial displacement in paths 2, 3, and 4 are earlier compared with path 1. Therefore, it is more appropriate to describe the radial flow with the increase of the radial displacement of the material inside the rivet shank, which is consistent with the previous research conclusion [36]. Careful observation shows that the radial deformation of rivet shank increases with the increase of hole diameter, especially when the hole diameter is 5.00 mm and 5.10 mm (see Fig. 8g ~ Fig. 8j). The main reason is that the reaction force of rivet by hole wall is reduced when the clearance between rivet and hole is increased, and the rivet shank is easier to be upset.

In this paper, the radial displacement value of path 2 is selected for research, and the radial displacement changes with the axial position under different hole diameters, as shown in Fig. 9. As can be seen, the position of radial displacement mutation will be later with the increase of squeeze force. The mutation point is located in the axial position of 5mm when the squeeze force is 15KN, as shown in Fig. 9a. However, when the squeeze force is 23KN, the mutation point is located in the axial position of 6mm, as shown in Fig. 9b. In other words, there will be more materials flow into the hole and the greater the expansion of the hole wall when the squeeze force increase, this is also consistent with the results of interference analysis. With the increase of the hole diameter, the material flowing into the hole increases slightly.

4.3 Effect of hole diameter on shear properties of riveted lap joints

The shear test results are shown in Fig. 10. The peak load of each specimen with different hole diameters can be obtained from the corresponding load-displacement curve. As the figure showed that the variation trend of the load-displacement curve is almost the same at different hole diameters. In the stage of loading, there is a parallel straight line segment of 0.1 mm, which is caused by the clamping slip of the joint and has no effect on the final shear force. Then, it enters the elastic deformation stage. In this stage, the rivet begins to deform with the increase of the tensile force until it finally breaks. This is mainly because the interference between the rivet and the hole becomes smaller when the squeeze force decreases, the rivet is easy to tilt in the hole under the action of tensile force, which will produce greater displacement when the rivet shank breaks. On the contrary, the diameter of the rivet shank increases with the increase of squeeze force, the rivet is not easy to tilt in the hole because the hole wall reacts on the rivet shank. In this case, the contact area between the rivet shank and hole wall will increases, so the bearing capacity is stronger.

To further illustrate the influence of hole diameter on the bearing capacity of riveted lap joints, the average value of shear force under the same parameters is taken as the graph, and the histogram of the influence of hole diameter on the shear force of riveted lap joints under different squeeze force is obtained, as shown in Fig. 11. The figure shows that the influence of the hole diameter on the shear force under different squeeze forces is consistent, the shear strength of the rivet increases with the increase of the hole diameter. It is noted that the deformation degree of the hole wall decreases with the increase of the hole diameter (see Fig. 7 and Fig. 9). At the same time, the rivet shank on the outer side of the sheet has more material flowing into the hole, and a larger rivet shank diameter can be obtained. The bearing strength of the riveted lap joints is usually determined by the diameter of the rivet shank. The larger the rivet shank diameter is, the larger the tensile force is needed to achieve the failure of the specimen, which means that the shear strength of the riveted lap joints increases with the increase of the hole diameter.

On the other hand, as Fig. 11 reveals that the shear strength of the specimen increases with the increase of squeeze force. Apparently, increasing the hole diameter can effectively improve the bearing strength of the riveted lap joints compared with increasing the squeeze force, which is contrary to the conclusion of Zeng [19]. The main reason is that the fatigue process is significantly different from the static load process, and the influencing factors of the fatigue process are more complex. Besides, the hole diameter in this paper is larger than the rivet diameter. However, three kinds of fit states were used in Zeng's research, including interference fit, transition fit, and clearance fit. Only from the point of view of improving the static strength, increasing the hole diameter is beneficial to improve the shear strength of the specimen. However, the fretting effect of fretting on the fatigue life of riveted lap joints can not be ignored in the process of service while pursuing high shear strength. It has been pointed out that the deformation of the hole wall decreases and the corresponding interference decreases with the increase of the hole diameter under the same squeeze force condition. Under cyclic load, cracks are easy to initiate from the hole edge for the sample with small interference, which eventually leads to the premature failure of the riveted lap joints [46]. However, some literature [47] shows that the effect of interference fit on fatigue life gain is weakened and even the fatigue life is reduced when the interference is too large. Therefore, choose the appropriate hole diameter can not only improve the bearing strength of the riveted

lap joints, but also improve the fatigue life. It is crucial to achieving the maximum benefit of the riveted lap joints.

Fig. 12 shows the effect of different hole diameters on the bearing capacity of the specimen. As the figure depicts the shear force of the specimen with a diameter of 4.90 mm, 4.94 mm, 5.00 mm, and 5.10 mm increases by 3.51%, 6.52%, 9.99%, and 17.77% respectively, compared with the specimen with a diameter of 4.82 mm under the condition of 15 KN squeeze force. When the squeeze force increases to 23 KN, the shear force of the specimen with a diameter of 4.90 mm, 4.94 mm, 5.00 mm, and 5.10 mm increases by 4.47%, 7.04%, 10.59%, and 17.24% respectively, compared with the specimen with a diameter of 4.82 mm. Except for the specimen with a diameter of 5.10 mm, the increased amplitude of shear force under the condition of 23 KN squeeze force is greater than that under the condition of 15 KN squeeze force.

4.4 Shear fracture analysis

In order to study the failure modes of riveted lap joints with different hole diameters, the macro characterization of the tested specimens was carried out. Fig. 13 shows the shear failure specimens of partially riveted lap joints under different combinations of hole diameter and squeeze force. For all the riveted specimens, the fracture occurs at the rivet shank of the interface of the laminate. There is no obvious necking phenomenon in all specimens, which indicates the brittle fracture of rivet under tensile force. It is worth mentioning that there is an obvious gap between the cross-section of the rivet shank and the hole wall, which is the result of the plastic deformation of the hole wall caused by the extrusion of the rivet shank. The plastic deformation zone can not recover after the fracture of the rivet shank, and the circular rivet hole is elongated to form an elliptical hole. Except for the deformation around the hole, the sheet has no obvious deformation. From the radial expansion diagram of the hole wall (see Fig. 7), a large interference step at the junction of the upper and lower sheets can be seen. Meanwhile, the single lap riveted joint is easy to produce secondary bending under the action of tensile force, and the out-of-plane deflection constraint is small, so the specimen breaks from the middle of the rivet shank. What's more interesting is that the rivet shank at rivet manufactured head-end stays in the outer sheet under the condition of 15 KN squeeze force, except that the rivet manufactured head of some specimens with a hole diameter of 5.10 mm fall off from the outer sheet, as shown in Fig. 13a. Different from the 15 KN squeeze force specimens, the rivet manufactured head of all specimens did not fall off from the outer sheet under 23 KN squeeze force, this is significantly different from specimens under the condition of 15 KN squeeze force. However, the rivet shank at the rivet driven head end of all shear specimens ejected from the hole under the condition of 15 KN squeeze force, regardless of the hole diameter. The above phenomenon was not observed under the condition of 23 KN squeeze force. The reason is that the interference close to rivet driven head under the condition of 23 KN squeeze force is larger than that 15 KN squeeze force. When the riveted lap joints are subjected to tensile force, the rivet shank squeezes the hole wall and makes the hole plastic deformation, forming a gap between the rivet shank and the hole. The specimens with small interference are not enough to offset the effect of the gap at the moment of fracture, so the rivet head falls off from the hole. The rivet manufactured head falls off from the outer sheet for the sample with a hole diameter of 5.10 mm, which is mainly because the extrusion of the rivet

shank on the outer side sheet becomes smaller when the hole diameter increases to 5.10 mm. It is estimated that if the hole diameter continues to increase, all rivet manufactured heads will fall off from the outer sheet.

Fig. 14 shows the macroscopic fracture morphology of the shear specimen under different combinations of hole diameter and squeeze force. As the figure shows, the shear failure position and fracture morphology are similar under different hole diameters and squeeze forces, which are the mixed mode of brittle and plastic fracture. The shear fracture of all specimens can be divided into zone 1 and zone 2. In the initial stage of shearing, there will be displacement between the upper sheet and the lower sheet under the action of shear force. In this case, the local stress concentration is easy to form in the rivet shank located at the interface of lamination. When the shear stress is much higher than the yield strength and fracture strength of the material, the crack at the fracture of zone 1 is generated and extended rapidly under the high stress, forming a shear band similar to brittle fracture. After that, the local stress concentration began to weaken, and the rivet began to change into the overall stress state. With the decrease of initial stress and enough time for crack propagation, the fracture mode changes from shear band to dimple, which is characterized by plastic fracture macroscopically. The area of zone 1 decreases with the increase of squeeze force under the same hole diameter, which means that the smaller the shear displacement when the rivet breaks, which can also be seen from the shear load-displacement curve.

Detailed micro fracture characteristics are shown in Fig. 15. Region 1 is a shear slip region, which is smooth and has obvious shear texture, and its direction is the same as the loading direction. Region 2 is relatively rough, goose down, and dark in color, which is an obvious plastic fracture zone. The aluminum alloy used in this paper belongs to the face-centered cubic structure. When the shear stress exceeds the critical shear stress, the crystal will slip along the direction of <1`1 0> and a slip shear band will be formed, as shown in Fig. 15c. With the increase of shear force, it will enter the transition zone from shear band fracture to ductile fracture. There is an obvious boundary in the transition zone that can be seen. The boundary is marked with a yellow dotted line, as shown in Fig. 15b. It is obvious that there are many elongated dimples along the direction of shear stress under the boundary of the slip zone, which is the result of plastic fracture of rivet shank. When the shear force exceeds the strength limit of the rivet shank, the bearing capacity of the rivet shank will be greatly reduced, and the rivet shank will be broken instantly. The area of region 1 is much smaller than that of region 2, which is different from the result of Li [32]. In the present research, the rivet material is aluminum alloy 2117-T4, while the rivet material is Q235 carbon steel in the experiment of Li. The tensile stress of Q235 carbon steel is larger than that of aluminum alloy 2117-T4. There is no doubt that Q235 has stronger resistance to tensile force deformation, so the area of region 1 is larger.

4.5 Shear failure mechanism

Fig. 16 shows the shear load-displacement curve of the typical shear specimen and the explanation of shear failure mechanism. According to the changing trend of the curve, the shear load-displacement curve can be divided into four stages, as shown in Fig. 16a. The first stage is called the adjustment stage.

In this stage, the gap between the fixture and the sample is adjusted under the action of tensile force. Meanwhile, the shear displacement and shear forces are very small, and the rivet and sheets are not deformed. The second stage is called the stationary stage. After the adjustment, the riveted lap joints enter the elastic stage. Due to the interference between the rivet and the sheets, the rivet is enough to resist the influence of the tensile force. The shear force and displacement increase linearly with the increase of tensile force, and the riveted lap joints have good stiffness characteristics at this stage. The third stage is called the degradation stage. With the further increase of the tensile force, the riveted lap joints enter the stage of plastic deformation, and the joint stiffness degrades continuously under the tensile force. In this stage, the lap sheets first yield and produce plastic deformation when the yield strength of the material around the hole is lower than the shear strength of the rivet, resulting in a gap at the interface between the rivet and the hole wall. Under the action of tensile force, the inner sheet and the outer sheet exert the same shear force and the opposite direction on the rivet shank, and finally the rivet tilts, which can be seen from Fig. 16b. As the tensile force continues to increase, the yield strength increases with the increase of the deformation degree of the sheets. The sheets stop deformation when the yield strength of the material around the hole is higher than the shear strength of the rivet, and the rivet is obviously damaged under the action of shear load, resulting in shear slip, as indicated in Fig. 15c. With the appearance of shear slip, the bearing capacity of the rivet shank is greatly reduced under the shear load, and the load drops sharply, resulting in fracture failure of the rivet shank. The shear force reaches the maximum at this stage.

5. Conclusion

The influence of different hole diameters on the shear properties of riveted lap joints was studied by finite element method and experiment in order to ensure the safety of service. Under the same squeeze force condition, different hole diameters have little effect on the dimension of rivet driven head. Therefore, it is limited to use the dimension of rivet driven head to evaluate the riveting quality. There is little difference in the expansion level of the outer sheet along the thickness direction under different hole diameters. The expansion degree of the hole wall on the side of the rivet driven head is greater than that on the side of the rivet manufactured head, whether it is 15 KN or 23 KN squeeze force. For all the riveted specimens, the fracture position occurs at the rivet shank of the interface of the laminate, and all the specimens are both brittle and plastic mixed fracture modes of rivet shank. There is an obvious gap between the rivet shank and the hole wall. The shear strength of the rivet increases with the increase of hole diameter. Compared with increasing the squeeze force, the shear strength of the riveted lap joints can be improved by increasing the hole diameter. Therefore, choose the appropriate hole diameter can not only improve the bearing strength of the riveted lap joints, but also improve the fatigue life. It is crucial to achieving the maximum benefit of the riveted lap joints. Under the condition of 15 KN squeeze force, the shear force of the specimen with a hole diameter of 4.90 mm, 4.94 mm, 5.00 mm, and 5.10 mm increases by 3.51%, 6.52%, 9.99%, and 17.77% respectively, compared with the specimen with a hole diameter of 4.82 mm. Under the condition of 23 KN squeeze force, the shear force of the specimen with a hole diameter of 4.90

mm, 4.94 mm, 5.00 mm, and 5.10 mm increases by 4.47%, 7.04%, 10.59%, and 17.24% respectively, compared with the specimen with a hole diameter of 4.82 mm.

Declarations

Acknowledgments

The authors are grateful to the support National Science Foundation of China (Grant No. 52005259), National Major Science and Technology Projects of China (Grant No. 2018ZX04014001) for sponsoring this project. Moreover, the authors would like to acknowledge the editors and the anonymous reviewers for their insightful comments.

Authors Contributions

Investigation: Ming Li, Wei Tian; Methodology: Ming Li, Wei Tian, Wenhe Liao; Test design and test execution: Ming Li, Junshan Hu; Software: Ming Li, Changrui Wang; Data analysis: Ming Li, Junshan Hu; Validation: Ming Li, Changrui Wang, Wenhe Liao; Writing-original draft preparation: Ming Li; Reviewing and editing: Ming Li, Wei Tian, Wenhe Liao; Funding acquisition: Wei Tian, Junshan Hu; Supervision: Wei Tian, Wenhe Liao;

Compliance with ethical standards

Conflict of interest The authors declare that there are no conflict of interest.

References

1. Manes, M. Giglio, F. Viganò, Effect of riveting process parameters on the local stress field of a T-joint. Int J Mech Sci. **53**(12), 1039-1049 (2011)
2. Zhang, H. Jiang, T. Luo, Theoretical and experimental investigation on interference fit in electromagnetic riveting. Int J Mech Sci. **156**, 261-271 (2019)
3. F. Zhang, H. Cheng, Y. Li, Riveting Process Modeling and Simulating for Deformation Analysis of Aircraft's Thin-walled Sheet-metal Parts. Chinese J Aeronaut. **24**(3), 369-377 (2011)
4. Skorupa, T. Machniewicz, A. Skorupa, Fatigue life predictions for riveted lap joints. Int J Fatigue. **94**, 41-57 (2017)
5. Zheng, H. Yu, X. Lai, Assembly deformation prediction of riveted panels by using equivalent mechanical model of riveting process. Int Journal Adv Manuf Tech. **92**(5-8), 1955-1966 (2017)
6. Jin, H. Wang, J. Tao, Effect of the interference fit on the stress distribution and failure mode of a flat-head riveted GLARE joint. Compos Struct. **235**, 111788 (2019)

7. Cao, Z. Cao, Y. Zhao, Damage progression and failure of single-lap thin-ply laminated composite bolted joints under quasi-static loading. Int J Mech Sci. **170**, 105360 (2019)
8. Taghizadeh, T.N. Chakherlou, Ghorbani H, Prediction of fatigue life in cold expanded fastener holes subjected to bolt tightening in Al alloy 7075-T6 sheet. Int J Mech Sci. **90**, 6-15 (2015)
9. Mohammadpour, T.N Chakherlou, Numerical and experimental study of an interference fitted joint using a large deformation Chaboche type combined isotropic–kinematic hardening law and mortar contact method. Int J Mech Sci. **106**, 297-318 (2016)
10. Li, K. Zhang, Y. Li, Influence of interference-fit size on bearing fatigue response of single-lap carbon fiber reinforced polymer/Ti alloy bolted joints. Tribol Int. **93**, 151-162 (2015)
11. Chishti, C.H. Wang, R.S. Thomson, Numerical analysis of damage progression and strength of countersunk composite joints. Compos Struct. **94**(2), 643-653 (2012)
12. Hu, K. Zhang, Y. Xu, Modeling on bearing behavior and damage evolution of single-lap bolted composite interference-fit joints. Compos Struct. **212**, 452-464 (2019)
13. Wan, Y. Huang, Friction stir welding of dissimilar aluminum alloys and steels: a review. Int Journal Adv Manuf Tech. **99**(5-8), 1781-1811 (2018)
14. Choudhury, T. Medhi, D. Sethi, Temperature distribution and residual stress in Friction Stir Welding process. Mater today. **26**, 2296-2301 (2020)
15. F.O. Braga, R. Maciel, L. Bergmann, Fatigue performance of hybrid overlap friction stir welding and adhesive bonding of an Al-Mg-Cu alloy. Fatigue Fract Eng M. **42**, 1262-1270 (2019)
16. J. Cui, S. Gao, H. Jiang, Adhesive bond-electromagnetic rivet hybrid joining technique for CFRP/Al structure: Process, design and property. Compos Struct. **244**, 112316 (2020)
17. Aman, S.H. Cheraghi, K.K. Krishnan, Study of the impact of riveting sequence, rivet pitch, and gap between sheets on the quality of riveted lap joints using finite element method. Int Journal Adv Manuf Tech. **67**(1-7), 545-562 (2013)
18. P. Szolwinski, T.N. Farris, Linking Riveting Process Parameters to the Fatigue Performance of Riveted Aircraft Structures. J Aircraft. **37**(1), 130-137 (2012)
19. Rijck, J.J. Homan, J. Schijve, The driven rivet head dimensions as an indication of the fatigue performance of aircraft lap joints. Int J Fatigue. **29**(12), 2208-2218 (2007)
20. H. Cheraghi, Effect of variations in the riveting process on the quality of riveted joints. Int Journal Adv Manuf Tech. **39**(11-12), 1144-1155 (2008)
21. Zheng, H. Yu, X. Lai, Assembly deformation prediction of riveted panels by using equivalent mechanical model of riveting process. Int Journal Adv Manuf Tech. **92**(5-8), 1955-1966 (2017)
22. Zeng, W. Tian, W.H. Liao, Improved Model Concerning Driven Rivet Head Dimensions Based on Material Flow Characteristics. Chinese J Aeronaut. **53**(4), 1-6 (2016)
23. Skorupa, T. Machniewicz, A. Skorupa, Fatigue life prediction model for riveted lap joints. Eng Fail Anal. **53**, 111-123 (2015)

24. Skorupa, T. Machniewicz, A. Skorupa, Fatigue strength reduction factors at rivet holes for aircraft fuselage lap joints. Int J Fatigue. **80**, 417-425 (2015)
25. Skorupa, A. Skorupa, T. Machniewicz, Effect of production variables on the fatigue behaviour of riveted lap joints. Int J Fatigue. **32**(7), 996-1003 (2010)
26. Elzbieta, S. Grzegorz, J. Jerzy, Comparison of the riveting process of a rivet with and without a compensator. Journal of Kones. **16**(4), 455-462 (2009)
27. F. Simenz, M.A. Steinberg, Alloy Needs and Design: The Airframe. Fundamental Aspects of Structural Alloy Design. (1977)
28. Wronicz, J. Kaniowski, B. Korzeniewski, Experimental and Numerical Study of Stress and Strain Field around the Rivet. (2011)
29. Rans, P.V. Straznicky, R. Alderliesten, Riveting process induced residual stresses around solid rivets in mechanical joints. J Aircraft. **44**(1), 323-329 (2007)
30. Skorupa, M. Skorupa, Riveted Lap Joints in Aircraft Fuselage[M]. Springer, Netherlands (2012)
31. R. Urban, Analysis of the fatigue life of riveted sheet metal helicopter airframe joints. Int J Fatigue. **25**(9-11), 1013-1026 (2003)
32. Li, J. Hao, Z. Xu, Mechanical properties and fatigue behavior of electromagnetic riveted lap joints influenced by shear loading. J Manuf Processes. **26**, 226-239 (2017)
33. G.A.A. Jaya, Safety risk in aircraft structural joints associated with the use of corrosion treatment. RMIT University, Australia (2013)
34. Atre, A Finite Element and Experimental Investigation on the Fatigue of Riveted Lap Joints in Aircraft Applications. Georgia Institute of Technology, America (2006)
35. Zeng, W.H. Liao, W. Tian, Influence of fit tolerance and squeeze force on the residual stress in a riveted lap joint. Int Journal Adv Manuf Tech. **81**(9-12), 1643-1656 (2015)
36. Zeng, J.T. Xue, X.Y. Liu, Design variables influencing the fatigue of Al 2024-T3 in riveted aircraft lap joints: Squeeze force and fit tolerance. Int J Fatigue. **140**, 105751 (2020)
37. P. Atre, W.S. Johnson, Analysis of the Effects of Interference and Sealant on Riveted Lap Joints. J Aircraft. **44**(2), 353-364 (2012)
38. Sławiński, T. Niezgoda, E. Szymczyk, J. Jachimowicz, Numerical study of the influence of shape imperfections on residual stress fields in a rivet hole. Journal of KONES. **17**, 427-434 (2010)
39. Li, G. Shi, N.C. Bellinger, Study of the Residual Strain in Lap Joints. J Aircraft. **43**(4), 1145-1151 (2006)
40. Zeng, W. Tian, X.Y. Liu, Experimental and numerical studies of stress/strain characteristics in riveted aircraft lap joints. J Mech Sci Technol. **33**(7), 3245-3255 (2019)
41. P.G. Muller, An experimental and analytical investigation on the fatigue behaviour of fuselage riveted lap joints. PhD thesis, Delft University of Technology, Netherlands (1995)
42. Liu, A. Zhao, Z. Ke, Influence of Rivet Diameter and Pitch on the Fatigue Performance of Riveted Lap Joints Based on Stress Distribution Analysis. Materials. **13**(16), 3625 (2020)

43. Blanchot, D. Alain, Riveted assembly modelling: Study and numerical characterisation of a riveting process. J Mater Process Tech. **180**(1-3), 201-209 (2006)
44. D. Rans, The role of rivet installation on the fatigue performance of riveted lap joints. PhD thesis, Carleton University, Canada (2007)
45. Y. Lei, Y.B. Bi, J.X. Li, Effect of riveting parameters on the quality of riveted aircraft structures with slug rivet. Adv Mech Eng. **9**(11), (2017)
46. Skorupa, M. Skorupa, T. Machniewicz, Fatigue crack location and fatigue life for riveted lap joints in aircraft fuselage. Int J Fatigue. **58**, 209-217 (2014)
47. N. Chakherlou, M. Mirzajanzadeh, J. Vogwell, Experimental and numerical investigations into the effect of an interference fit on the fatigue life of double shear lap joints. Eng Fail Anal. **16**(7), 2066-2080 (2009)

Figures

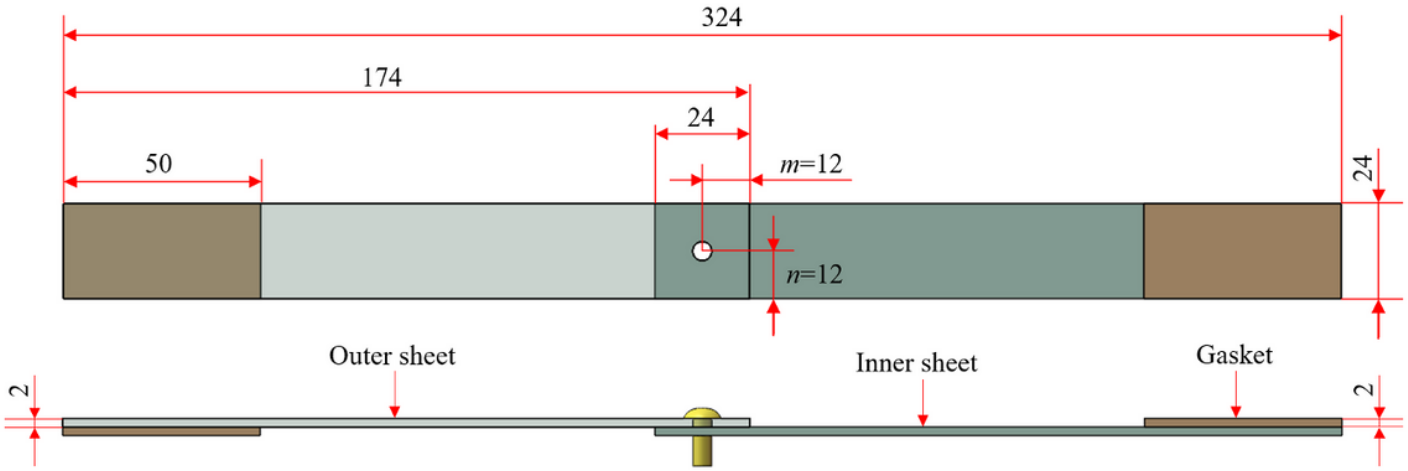

Figure 1

Dimensions of the experimental test specimens (mm)

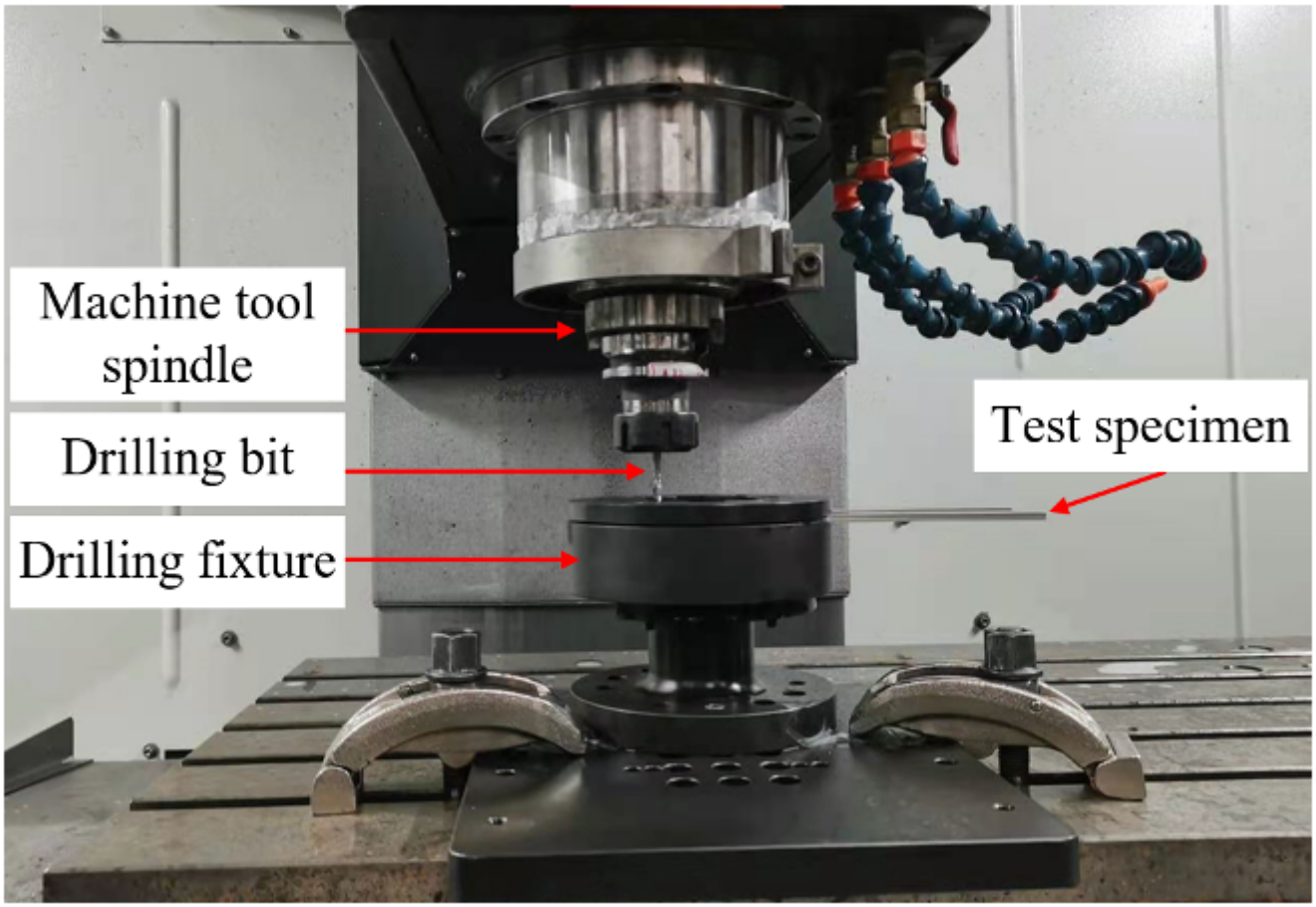

Figure 2

Drilling experiment platform

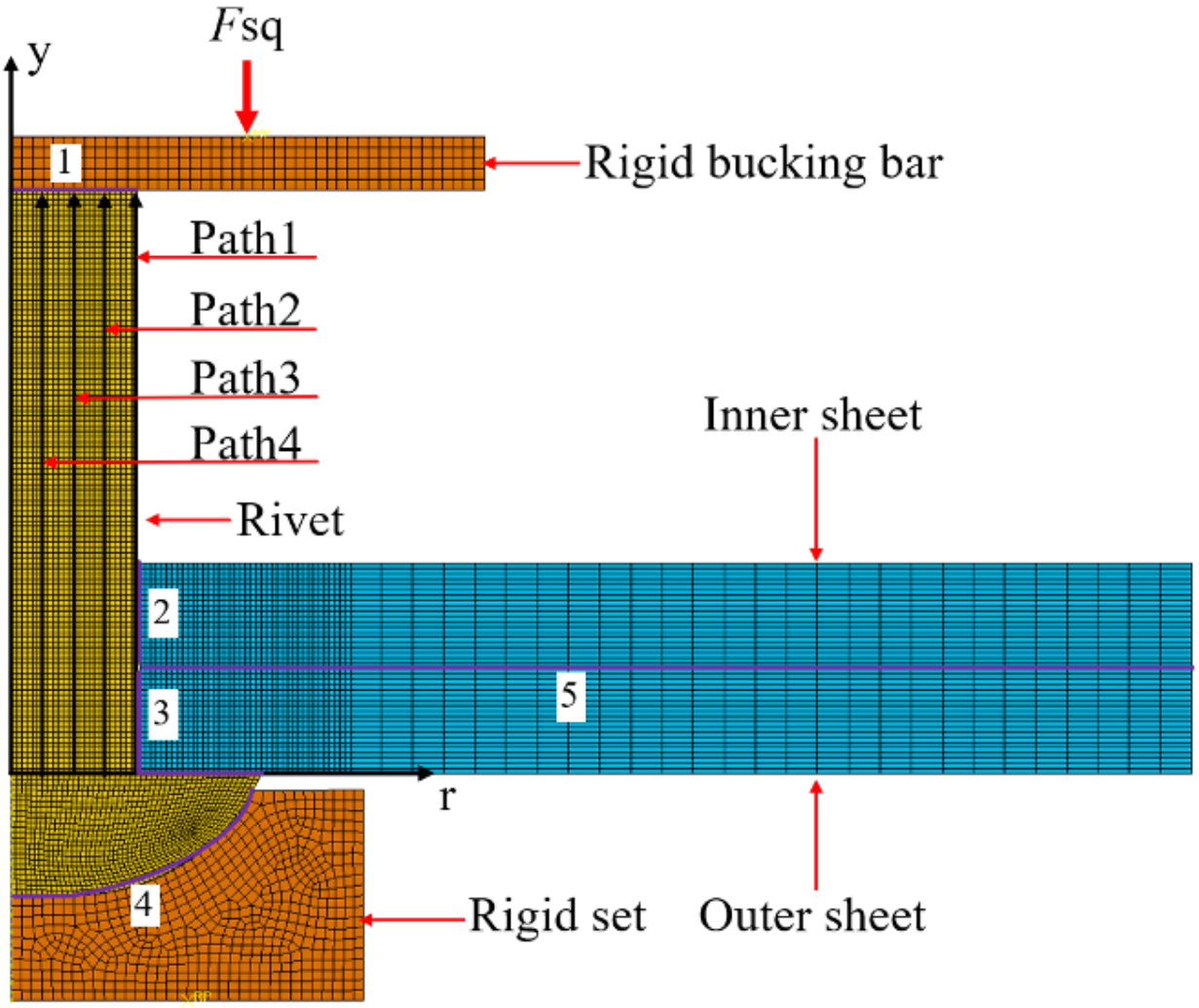

Figure 3

2D axisymmetric finite element mesh model

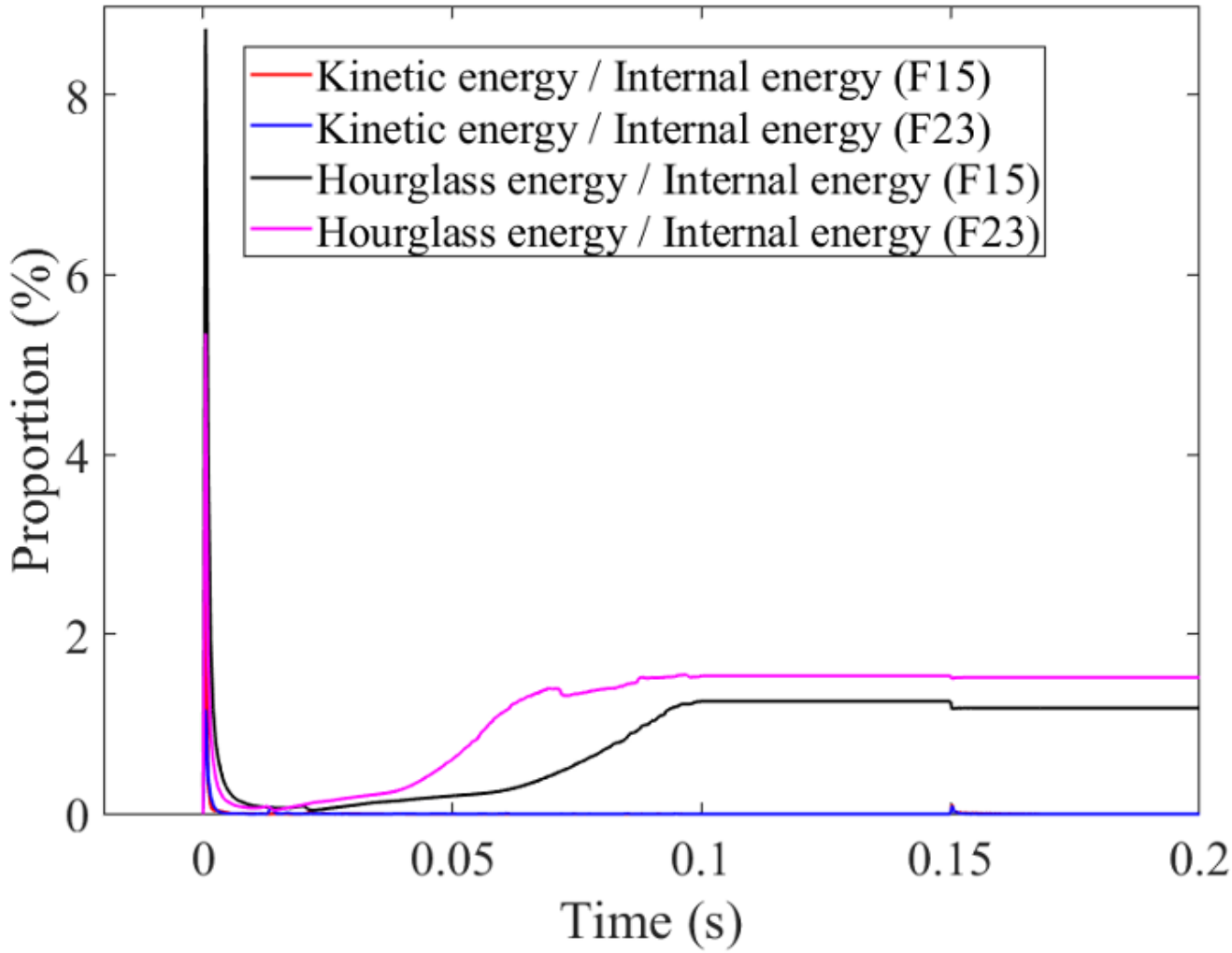

Figure 4

Energy analysis of the riveting process

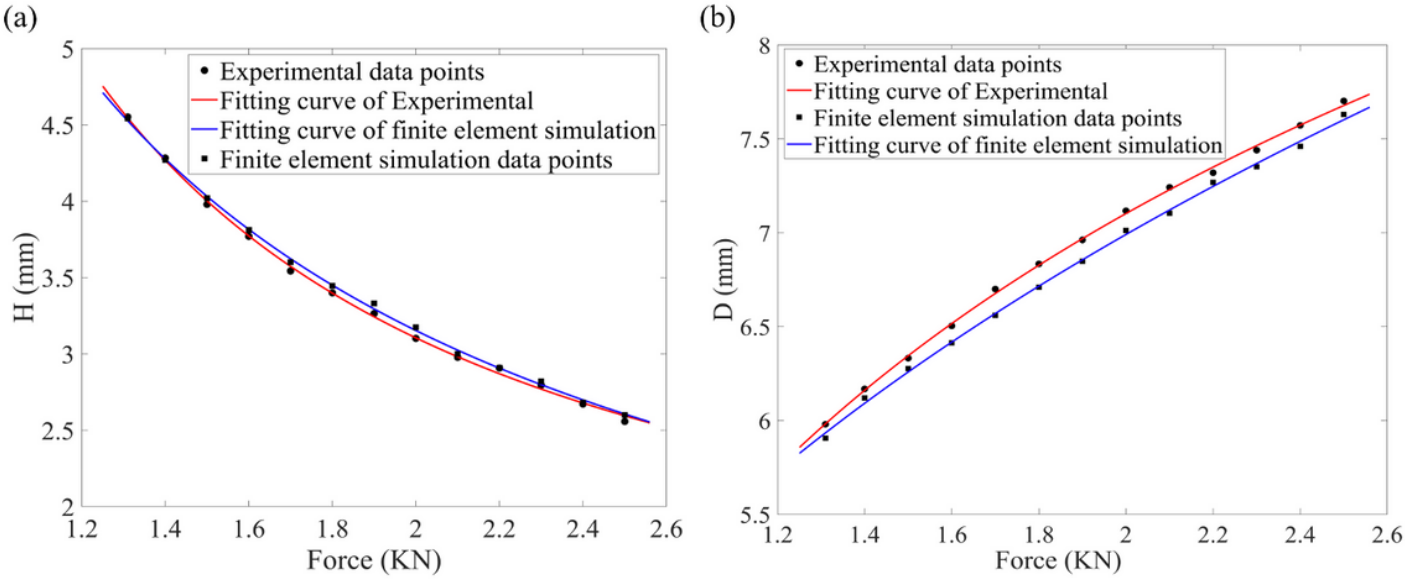

Figure 5

Comparison of experimental results and finite element simulation results: a Height of driving head; b Diameter of driving head

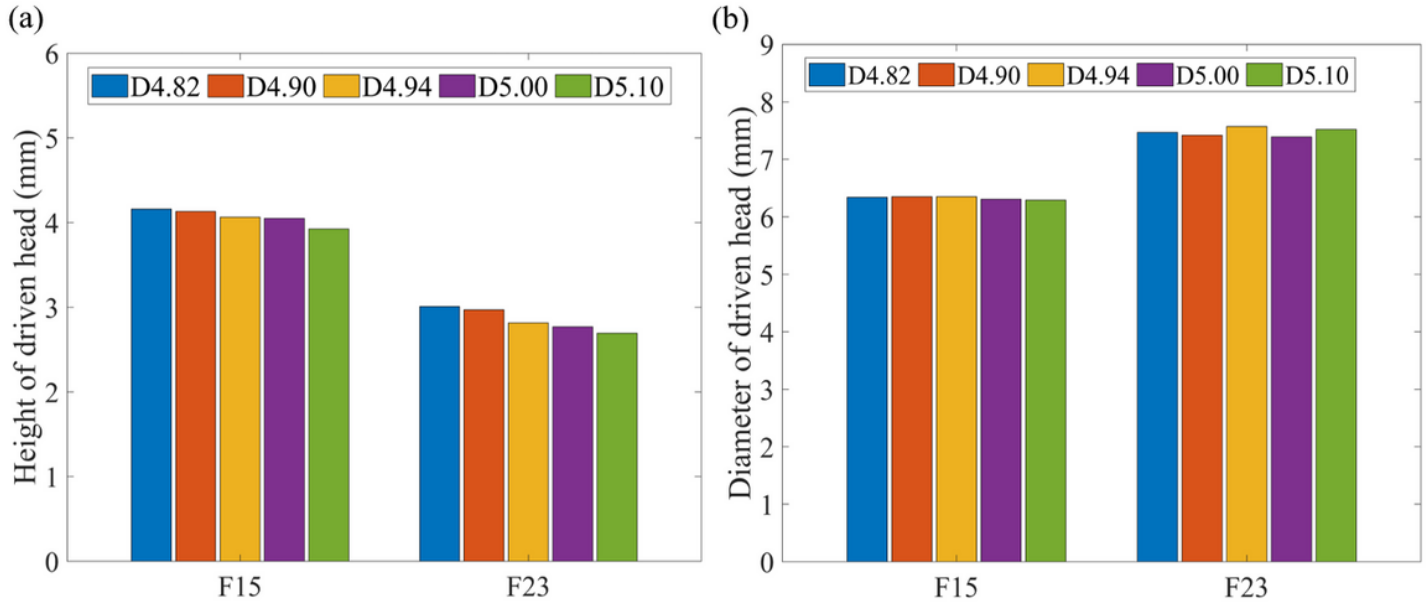

Figure 6

Variation of rivet driven head dimension with hole diameter under different squeeze force: a Height of driven head; b Diameter of driven head

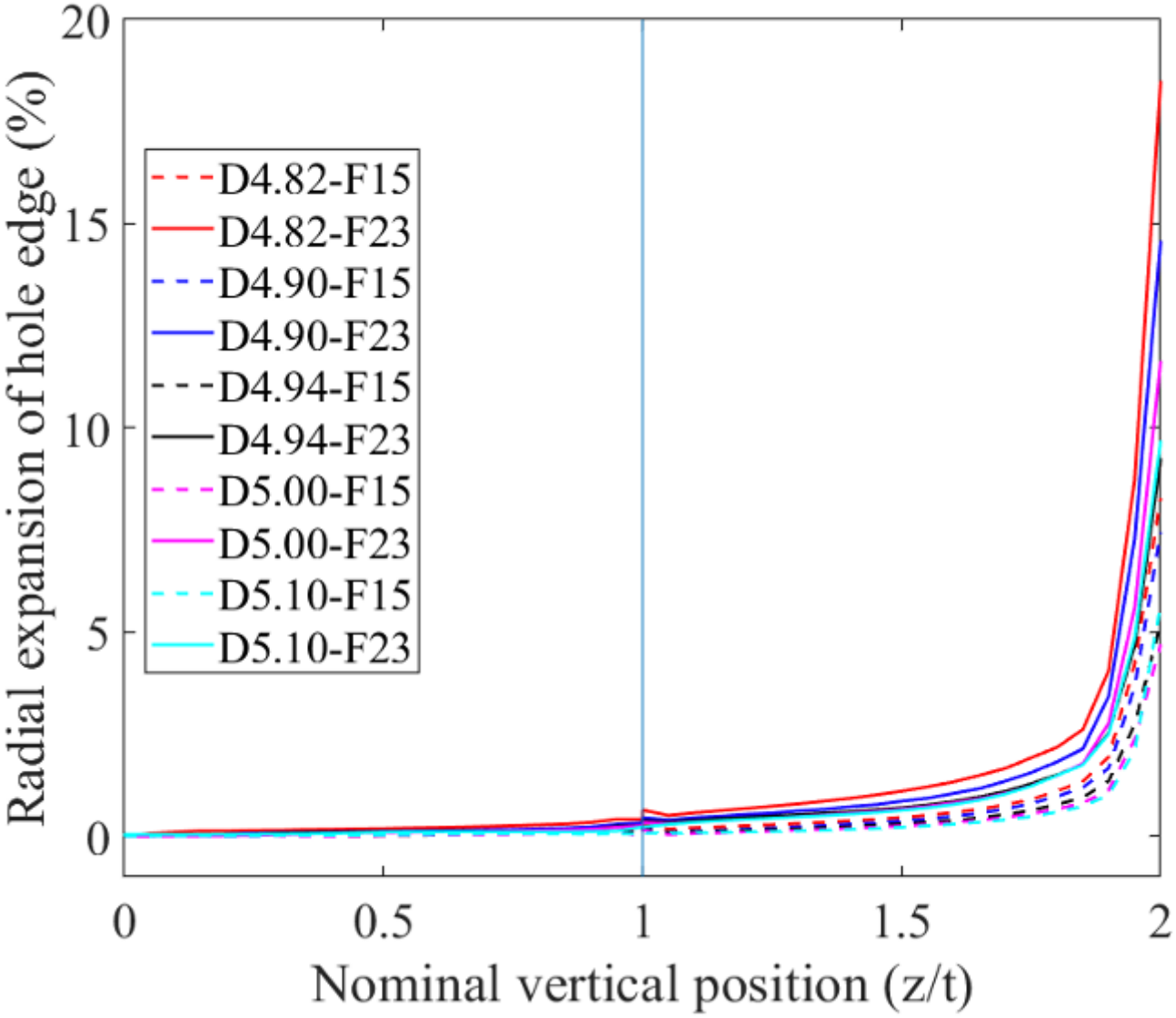

Figure 7

Radial expansion of rivet holes with different hole diameters at various squeeze forces

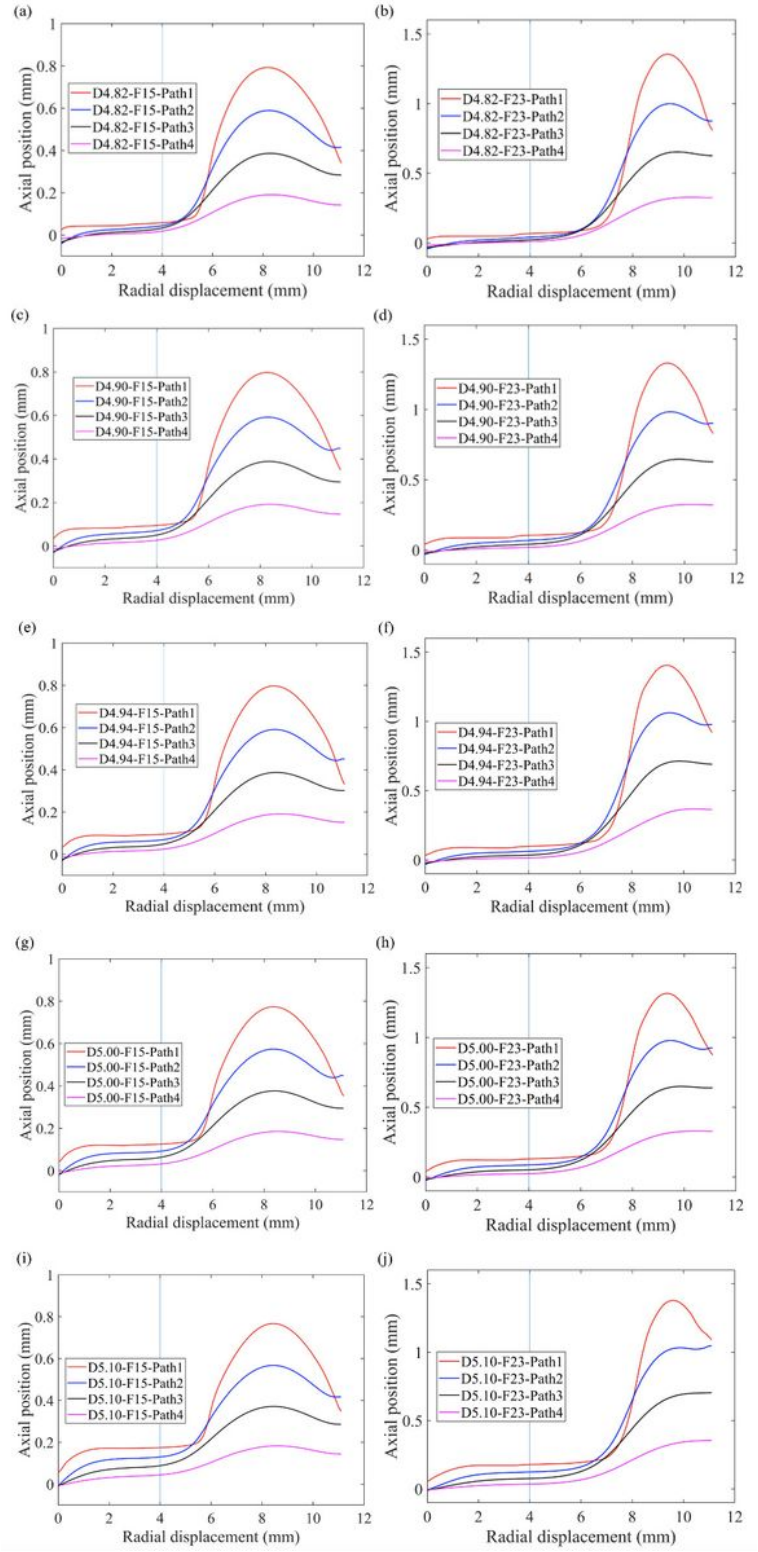

Figure 8

The radial displacement changes with the axial position: a D4.82-F15; b D4.82-F23; c D4.90-F23; d D4.90-F23; e D4.94-F23; f D4.94-F23; g D5.00-F23; h D5.00-F23 ;i D5.10-F23; j D5.10-F23

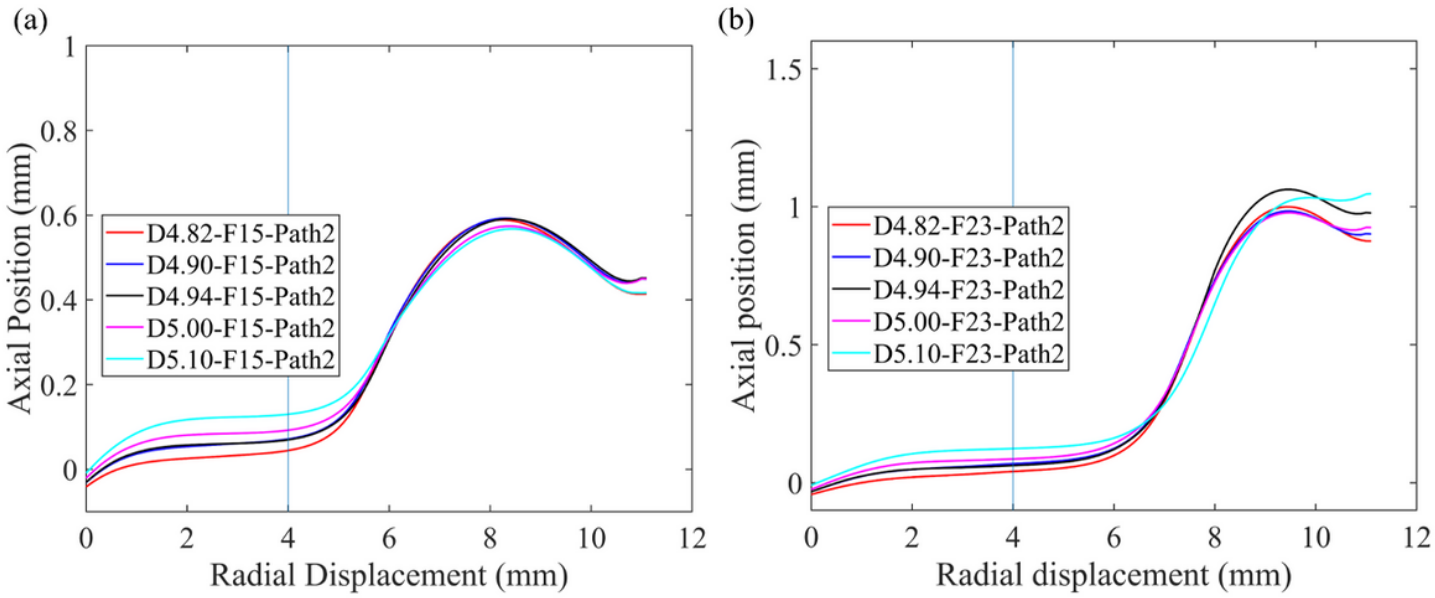

Figure 9

The radial displacement changes with the axial position under different diameters of path 2: a 15 KN; b 23 KN

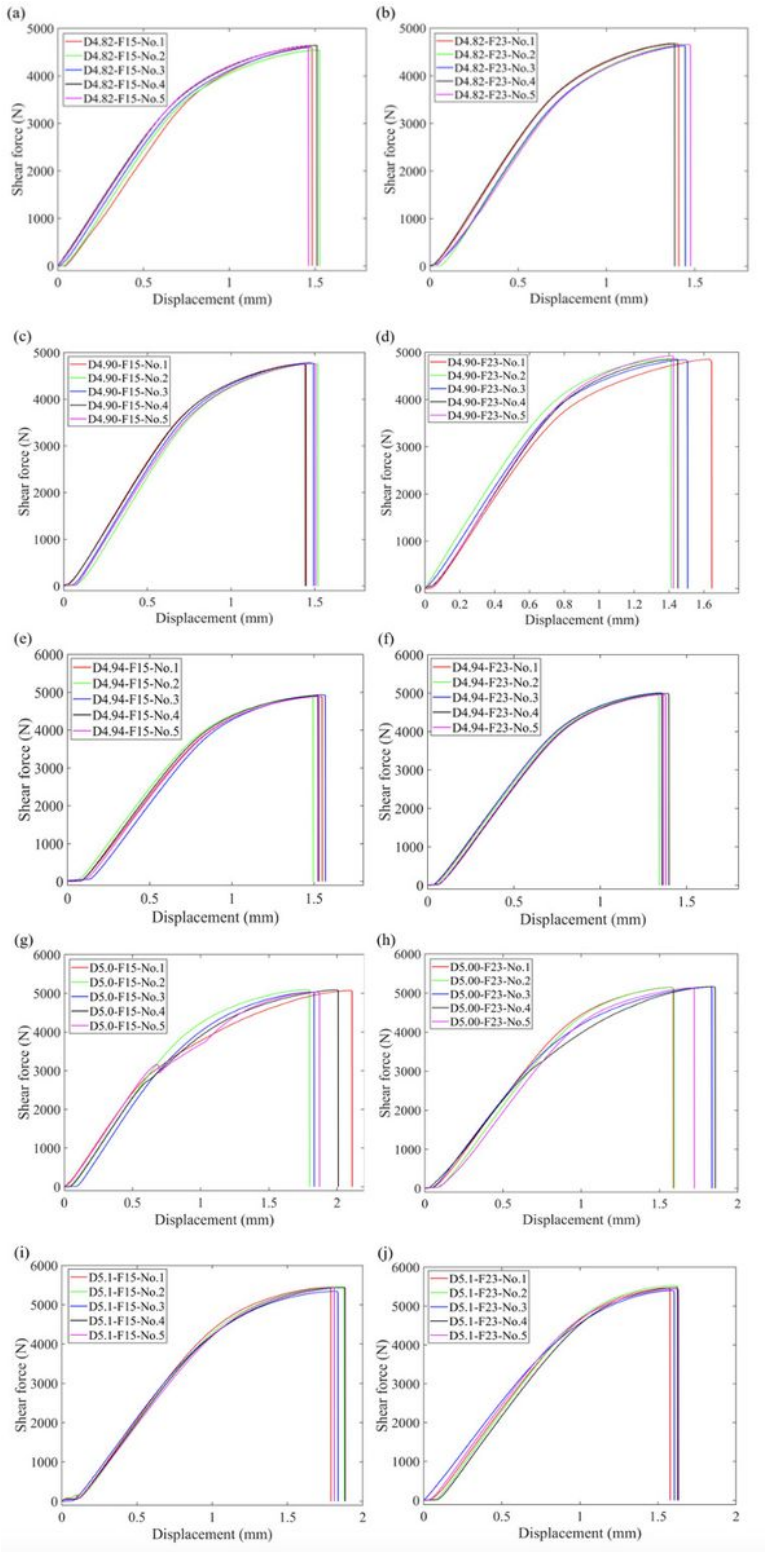

Figure 10

Relationship between shear force and displacement: a D4.82-F15; b D4.82-F23; c D4.90-F15; d D4.90-F23; e D4.94-F15; f D4.94-F23; g D5.00-F15; h D5.00-F23; i D5.10-F15; j D5.10-F23

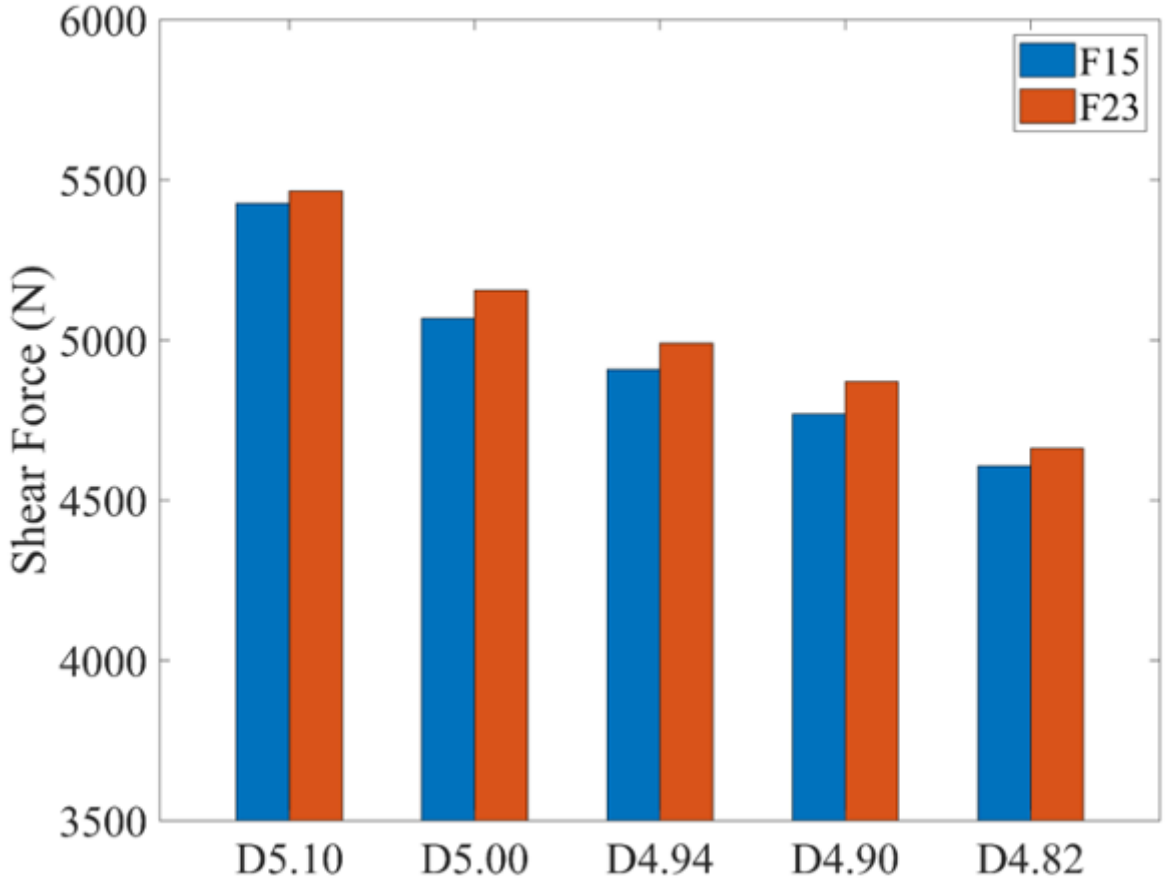

Figure 11

Mean value of shear force under different hole diameters

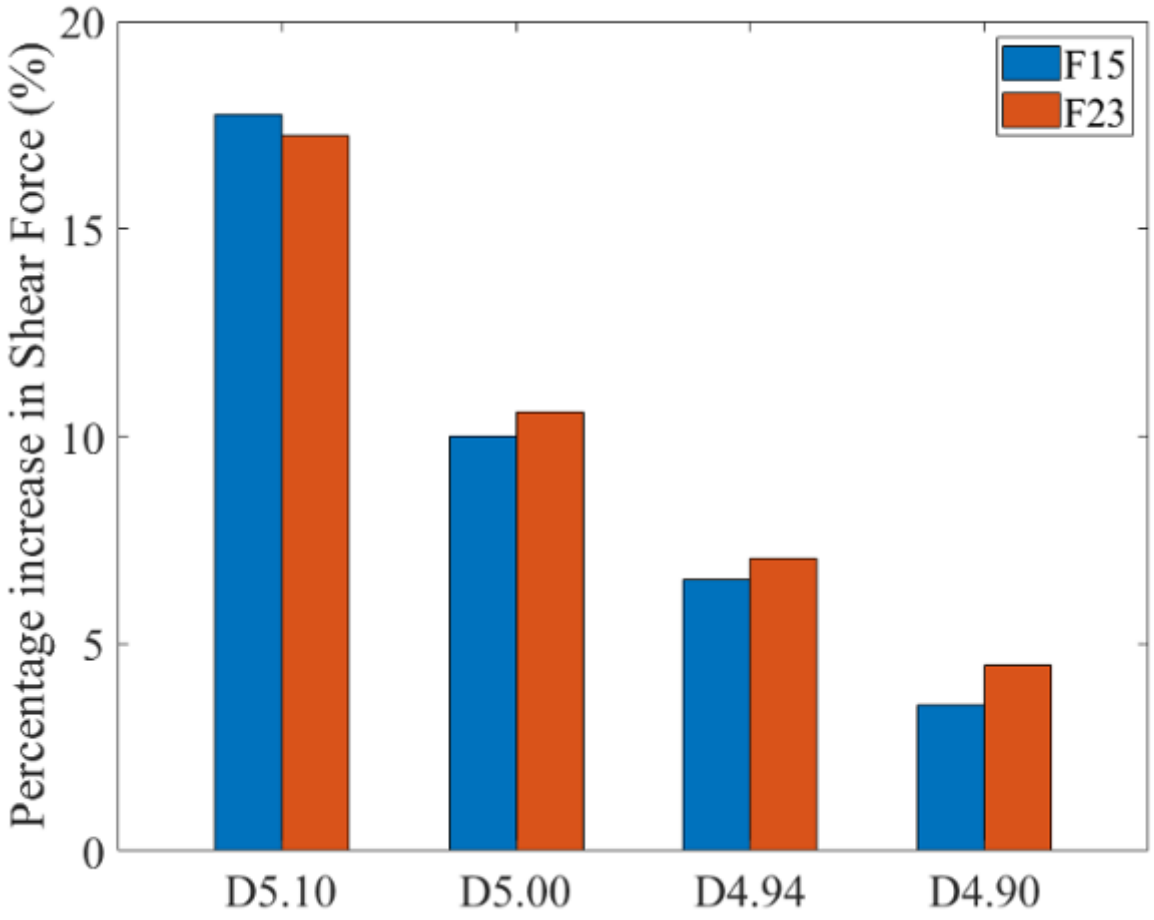

Figure 12

Percentage increase of shear force under different hole diameters

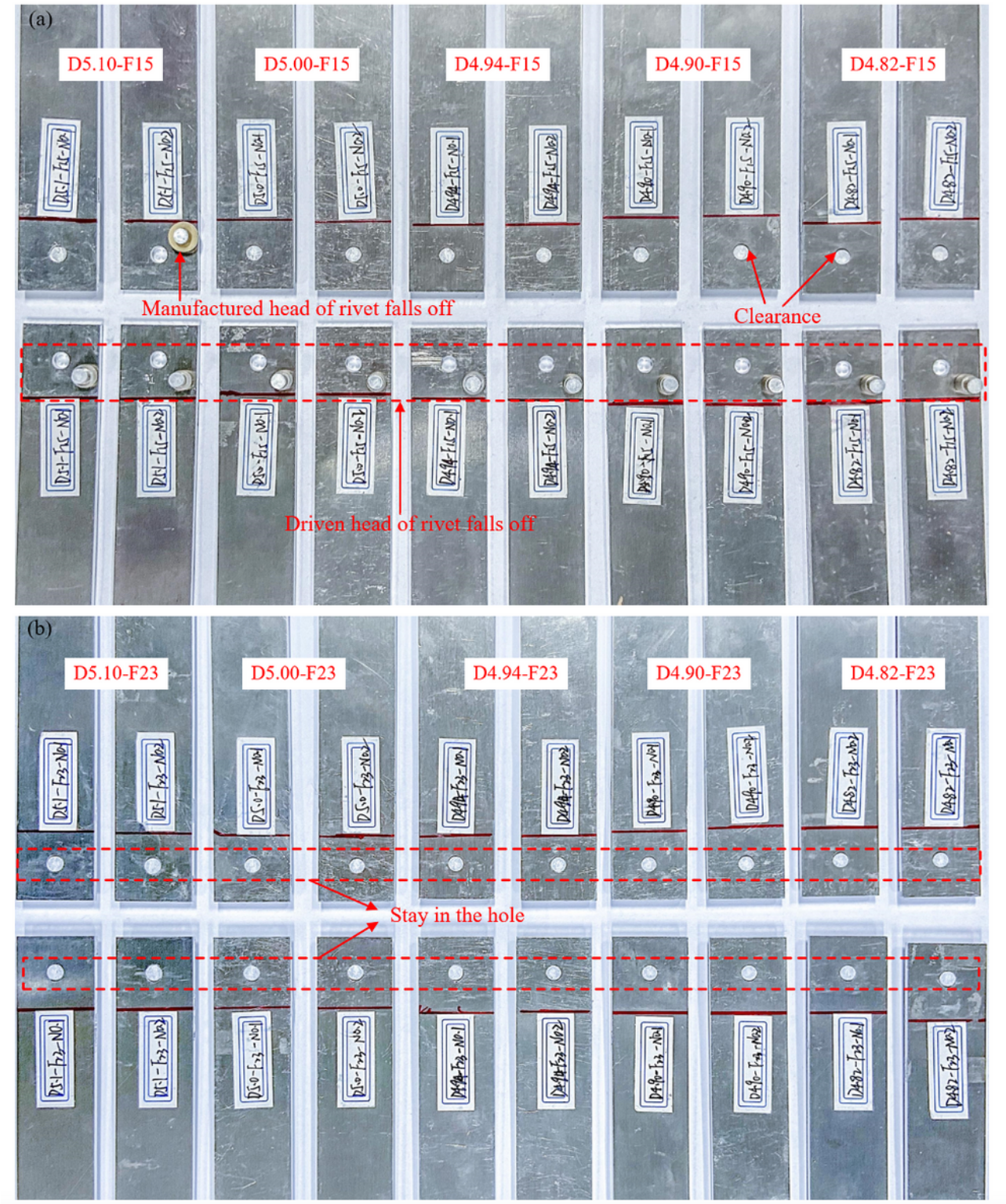

Figure 13

Macrograph of shear failed specimens for the investigated riveted lap joints: a 15 KN; b 23 KN

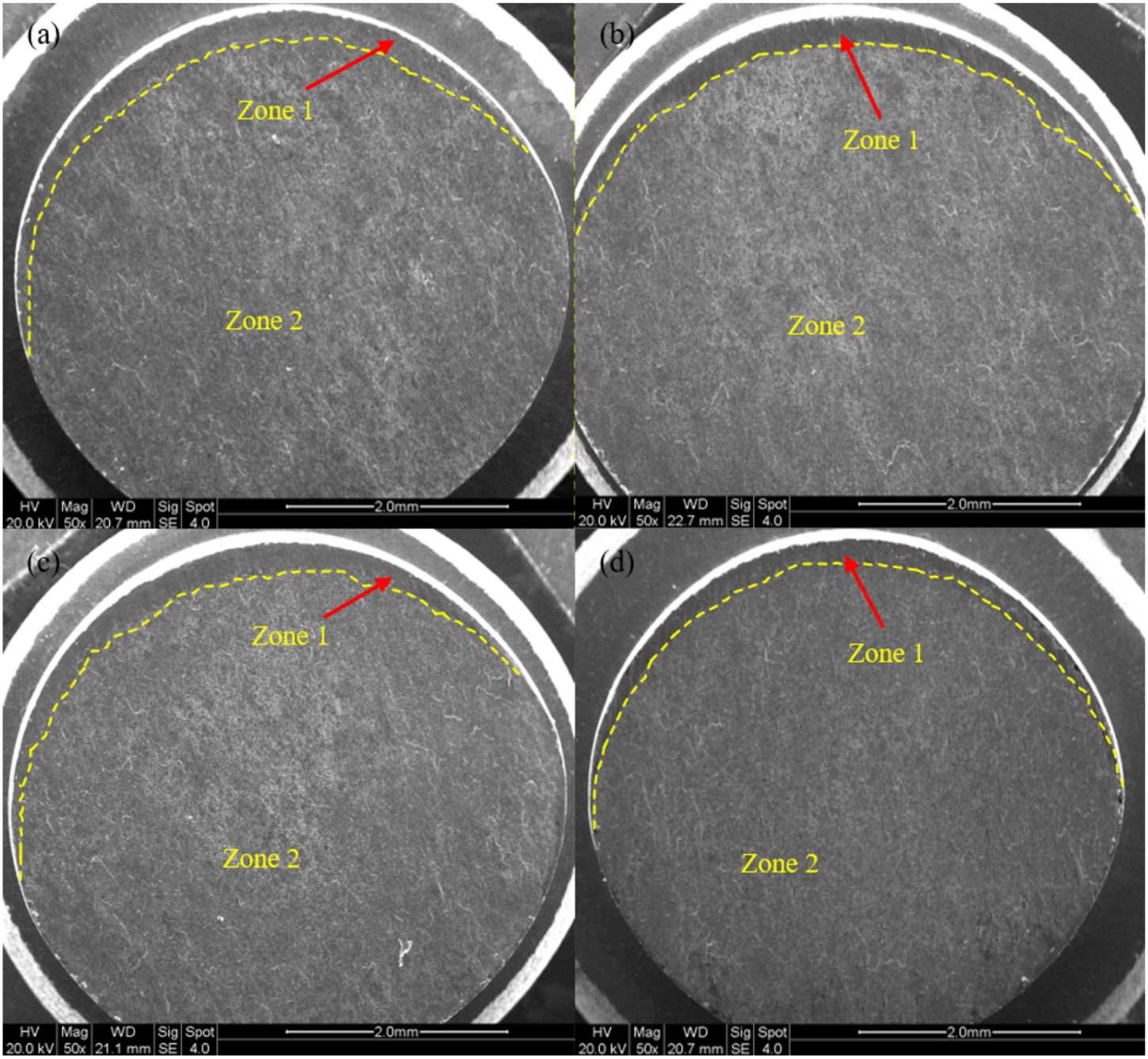

Figure 14

Macroscopic fracture morphology of shear specimen: a D4.90-F15; b D4.90-F23; c D5.10-F15; d D5.10-F23

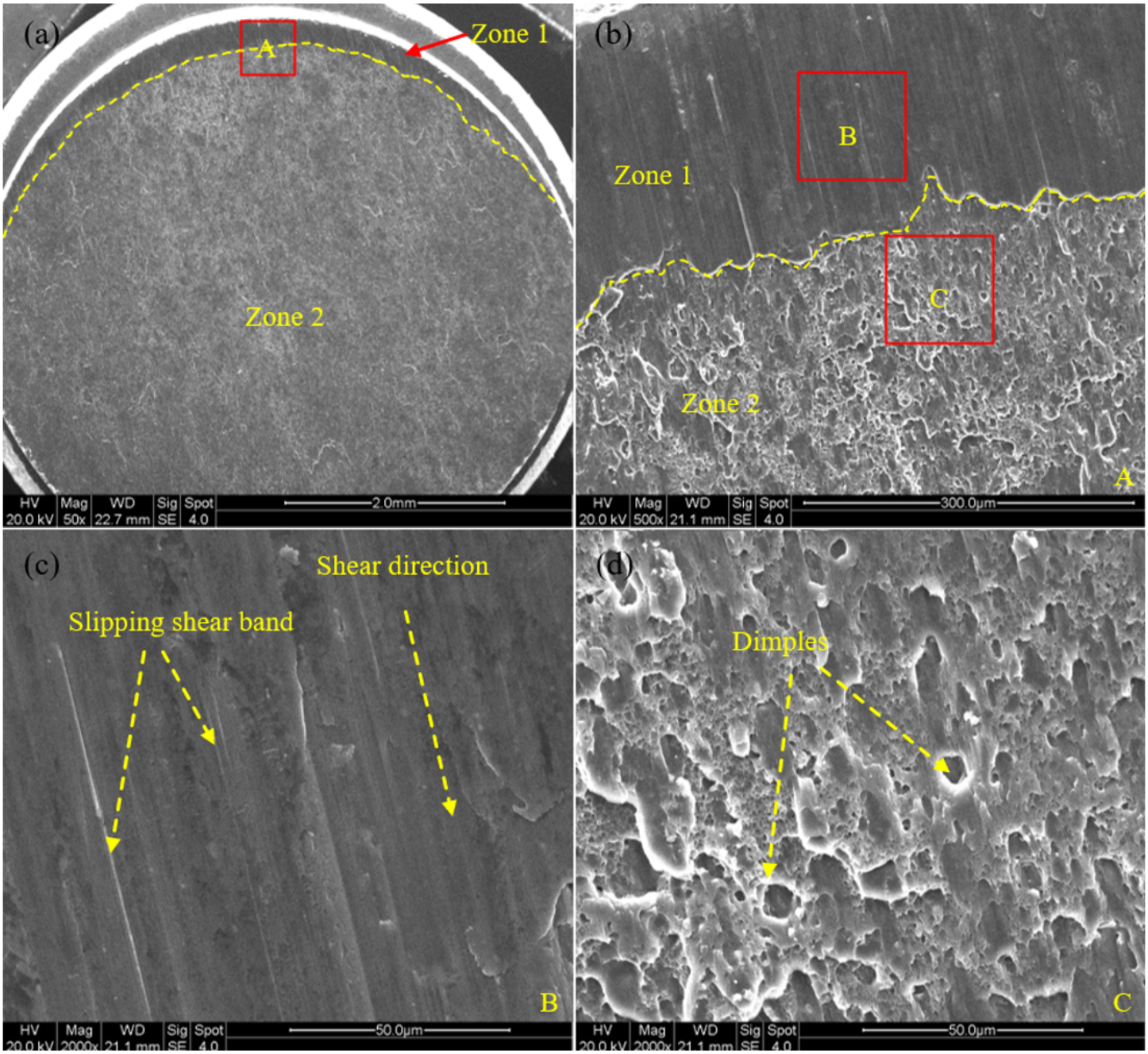

Figure 15

Microfracture characteristics of typical specimens: a Macro fracture; b Magnified area A; c Magnified area B; d Magnified area C

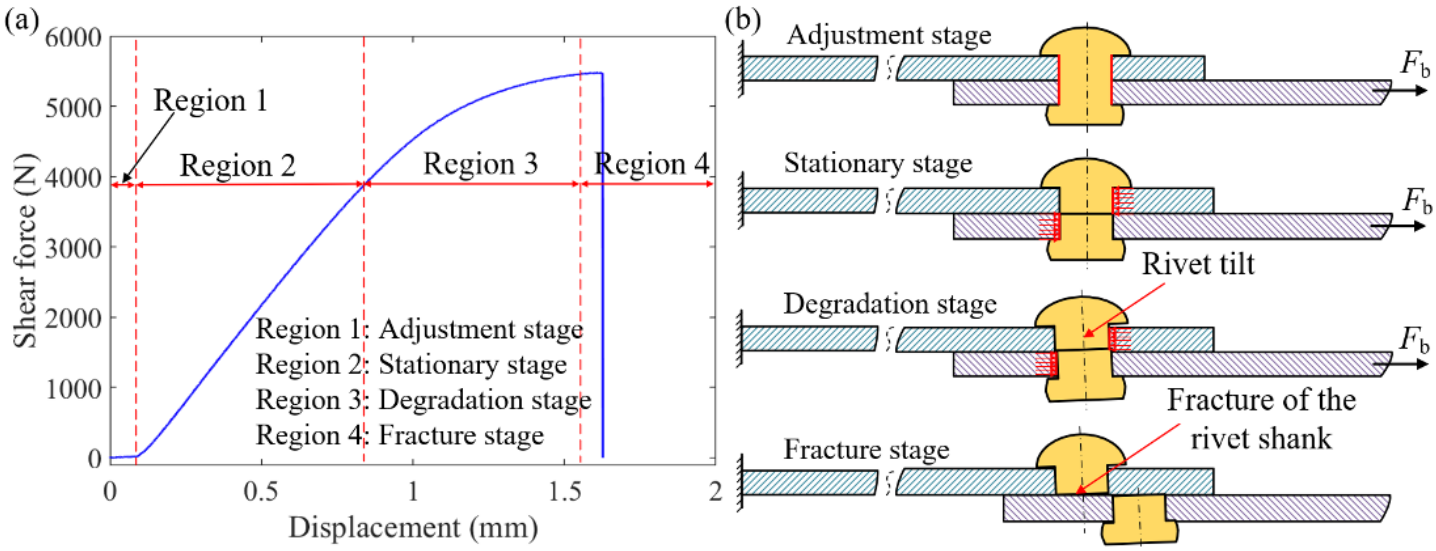

Figure 16

Description of typical load displacement curve and shear failure mechanism: a Load-displacement curve; b Shear failure mechanism